Detonation in ammonia-oxygen and ammonia-nitrous oxide mixtures

Zifeng Weng, Rémy Mével, Nabiha Chaumeix

Detonation in Ammonia-Oxygen and Ammonia-Nitrous Oxide Mixtures

Zifeng Weng[a], Rémy Mével[a], Nabiha Chaumeix[b]

[a]*Center for Combustion Energy, School of Vehicle and Mobility, Tsinghua University, 30 Shuang Qing road, 100084, Beijing, China*
[b]*Institut de Combustion, Aerothermique, Reactivite et Environnement, CNRS-ICARE, Orleans, 45000, France*

Abstract

The sensitivity to detonation of ammonia-oxygen (NH_3-O_2) and ammonia-nitrous oxide (NH_3-N_2O) mixtures has been investigated experimentally and numerically. Detonation were studied in a stainless tube with a length of 4.6 m and an inner diameter of 78 mm. The initiation of the detonation wave was achieved using a weak electric spark and a Shchelkin spiral to trigger flame acceleration and transition to detonation. The soot foil technique was employed to determine the detonation sensitivity. For the numerical simulations, the Shock and Detonation Toolbox in Cantera was employed. The pressure in experiment was below 100 kPa and was extended to 4.5 MPa in the numerical study using a real gas model based on the Peng-Robinson equation of state. Overall, detonation in ammonia-based mixtures have an irregular structure and do not demonstrate a high sensitivity. At ambient temperature, the experimental cell width ranges between 14 and 54 mm for NH_3-O_2 mixtures and between 7 and 23 mm for NH_3-N_2O mixtures in the equivalence ratio and pressure ranges ϕ=0.6-1.5, and P_1=43-100 kPa, and ϕ=0.3-1.25, and P_1=41-80 kPa, respectively. These cell widths are larger than for CH_4-O_2 mixtures under similar conditions. The mixture with N_2O is more sensitive to detonation at low pressure, but the conclusion is opposite at elevated pressure. Increasing pressure also tends to stabilize the detonation by raising the isentropic coefficient. Through detailed thermochemical analysis, it was shown that detonation in ammonia-based mixtures show pathological detonation behaviour at low pressure. The major exother-

Email address: mevel@mail.tsinghua.edu.cn (Rémy Mével)

mic reaction is $NH_3 + OH = NH_2 + H_2O$ in NH_3-O_2 but it is outweighed by $H + N_2O = N_2 + OH$ in NH_3-N_2O mixture. One of the dominant radicals is OH, which is supplied by $H + O_2 = O + OH$ at low pressure and by H_2O_2 (+M) = 2OH (+M) at elevated pressure in NH_3-O_2 mixture; and by $H + N_2O = N_2 + OH$ in NH_3-N_2O mixture. The characteristic length scale, i.e., the induction distance, is sensitive to reactions responsible for supplying OH radical in both mixtures. In NH_3-N_2O mixture, the induction distance is also sensitive to reactions involving the oxidizer, N_2O.

Keywords: Ammonia, Safety, Detonation structure, Cell width, Real gas effects

---

Nomenclature

Abbreviation

CJ	Chapman-Jouguet
DDT	Deflagration to detonation transition
EoS	Equation of state
IG	Ideal gas
PR	Peng-Robinson
RoP	Rate of progress
vdW	van der Waals
ZND	Zel'dovich-von Neumann-Döering

Physical constants

k_B	Boltzman constant (J/K)
R	Universal gas constant (J/K/kmol)

Quantities

$\bar{H}_k$	Partial molar enthalpy of species k (J/kmol)
β'	Coefficient of thermal expansion (K^{-1})

β_s	Isentropic coefficient
χ	The χ stability parameter
ΔG^0	Gibbs free energy of reaction (J/kmol)
Δ_i	Induction zone length (m)
$\dot{\sigma}$	Thermicity (s^{-1})
η	$1 - M^2$, the sonic parameter
γ	Heat capacity ratio
λ	Cell width (m)
$\mathbf{Y}$	Vector of Mass fraction
ω	Acentric factor
$\overline{k}_{ij}$	Binary interaction coefficient between species i and j
ϕ	Equivalence ratio
ϕ_k	Fugacity coefficient of species k
ρ	Density (kg/m^3)
σ_d	Molecule diameter (m)
τ	Induction time (s)
θ	Reduced activation energy
ε	Well depth (J)
φ_1, φ_2	Constants for distinguishing different EoS
a	Molecular attraction parameter of mixture (Pa $m^6/kmol^2$)
b	Covolume parameter of mixture (m^3/kmol)
c_p	Constant pressure heat capacity, (J/kg/K)
c_v	Constant volume heat capacity, (J/kg/K)
D_{CJ}	Chapman-Jouguet speed (m/s)

K_c Equilibrium constant ($(\text{kmol/m}^3)^{\sum_{k=1}^{K} v_{k,i}}$)

$k_{f,i}$, $k_{r,i}$ Forward and reversed reaction rate constant of the ith reaction (Unit: a combination of kmol, m^3 and s)

M Mach number

P Pressure (Pa)

r Net reaction rate (kmol/m^3/s)

S_i Sensitivity coefficient of the ith reaction

T Temperature (K)

t Time (s)

T_r Reduced temperature, T/T_c

V Volume (m^3/kmol)

$v_{k,i}$ $v''_{k,i} - v'_{k,i}$

$v''_{k,i}$ Stoichiometric coefficient of species k as a product in reaction i

$v'_{k,i}$ Stoichiometric coefficient of species k as a reactant in reaction i

w Velocity in the shock attached coordinate (m/s)

X Mole fraction

y Mass fraction

Z Compressibility factor

$\bar{V}_k$ Partial molar volume of species k (m^3/kmol)

Subscript

$+1, -1$ Perturbation by increasing or decreasing the detonation speed by 1%

c Critical property

i, j, or k The i^{th}, j^{th}, or k^{th} species or reaction

vN von Neumann state

max Maximum value

1. Introduction

Ammonia is a promising fuel to achieve zero carbon emission. Compared to hydrogen, ammonia has high energy density and good compatibility with the existing technologies and infrastructure [1, 2]. It can be liquefied at a much lower pressure than the one required for hydrogen, which makes the storage of ammonia much more efficient and cost effective than the storage of hydrogen [1]. The high potential of ammonia as an energy vector has motivated many fundamental studies on its combustion properties. For example, (i) the laminar flame speed of ammonia-based mixtures has been studied by [3, 4, 5]; (ii) shock-tube and rapid compression machine experiments have been performed to determine the auto-ignition delay-time [6, 7, 8, 9]; (iii) the combustion or pyrolysis of ammonia in micro-flow reactor and flow reactor have also been investigated [10, 11, 12, 13]; and (iv) detailed reaction models to describe ammonia combustion under various conditions have been proposed [14, 15, 16, 17, 18]. In general, ammonia-air mixtures demonstrate low reactivity with very low laminar flame speed; long ignition delay-time; and high ignition temperature. Further details, including comprehensive discussion of chemical kinetics and reaction rate constants relevant to ammonia combustion, can be found in recent review articles [2, 19, 20].

The main risks associated with ammonia are related to its corrosive nature and its high toxicity [20]. The risk of vapor explosions has been studied but the risk of accidental combustion is considered to be low because of the high ignition energy and low laminar flame speed [20]. Despite this aspect, it is noted that limited data are available on flame acceleration, transition to detonation, and detonation for such mixtures. Thomas [21] studied deflagration to detonation transition (DDT) in methane-ammonia-oxygen mixtures. The methane to ammonia ratio was 1 and 1.176. The effects of the initial pressure (P_1), initial temperature (T_1), and O_2 content were studied using the following ranges: P_1=50-7000 kPa; T_1=293-540 K; and X_{O2}=0.33-0.45. No detonation was observed for O_2 content below 40%. In most cases, initial pressure above atmospheric was required to induce violent pressure transient/variation. Using chemical kinetics simulations and considering a linear relationship between the induction zone length (Δ_i) and the cell width (λ), the detonation cell width of these mixtures was predicted to be in the range 10-220 mm over the range of conditions previously reported. Flame acceleration and DDT for a NH_3-H_2-air (13/12/75 %) mixture was studied by Thomas et al. [22], in which weak acceleration and no DDT were ob-

served. More recently, Jing et al. [23] studied flame acceleration and DDT in ammonia-oxygen mixtures for equivalence ratio ϕ = 0.3-2.2 at ambient temperature and pressure. The inner diameter of the detonation tube was 0.093 m. Ignition was achieved using an electric spark of up to 40 J. For the stoichiometric mixture, the DDT run-up distance was 5.05 m whereas the distance required to form a self-sustained Chapman-Jouguet (CJ) detonation was around 8 m. While DDT was observed over the range ϕ=0.6-2.2, no self-sustained detonation could be observed at ϕ=2.2. Maximum pressure peak in the range 2.7-3 MPa were measured and seem consistent with the CJ theory. From Jing et al.'s work, it is also noted that the over-pressure generated by ammonia-oxygen mixtures is higher than that generated by H_2-O_2 mixtures, approximately 1.8 MPa. In the detonation database of Kaneshige and Shepherd [24], no minimum tube diameter (smallest tube diameter for which a self-sustained detonation can propagate [25]), critical energy (minimum energy required to initiate directly a detonation using a point energy source [26, 27]), nor critical tube diameter (smallest tube allowing the successful transmission of a planar detonation to an unconfined space [28, 29]) data are available for ammonia. Only few cell width data are provided by Akbar et al. [30]. They were obtained for ammonia mixed with either oxygen, or with nitrous oxide, or with nitrous oxide and air, and cover the following ranges of conditions: ϕ=0.56-1; P_1=55-91 kPa; T_1=293 K; and $X_{N2/air}$=0-0.533. Although all these data have been generated, it is clear that more are needed to avoid compromising the accuracy of the fundamental background of this subject and the safe utilization of ammonia. In addition, potential development of detonation engines fueled with ammonia-based mixtures is compromised by such a lack of knowledge of the detonation parameters.

It is noted that ammonia demonstrates a particularly strong real gas behavior even at relatively low pressure as seen for example from the compressibility factor diagram shown in [31]. The critical temperature and pressure of pure ammonia are 405.4 K and 11.353 MPa, respectively. Both of them are much higher than the corresponding critical properties of hydrogen and hydrocarbon fuels. At ambient temperature and elevated pressure, ammonia has a compressibility factor less than 1 and the state is close to the critical state, which leads to relatively strong real gas effect. Real gas effect on detonation has been studied for a variety of mixtures including hydrogen-based (H_2-O_2 and H_2-air) and hydrocarbon-based (CH_4-O_2(-N_2), C_2H_6-O_2-N_2, C_2H_4-O_2-N_2, and C_3H_8-O_2-N_2) mixtures. Experimental measurements of the detonation velocity and detonation cell width in high-pressure gases

were performed by Gealer et al. [32] and Bauer et al. [33]. The use of non-ideal equation of state (EoS) was found to given accurate prediction on the detonation speed [34]. More recently, Taileb et al. [35] studied the effect of real gas on the two-dimensional structure of detonation using a 1-step reaction model. They found that the cellular structure was more regular when accounting for real gas effects. The above studies have shown that real gas effects may be observed for initial pressure as low as 1 MPa [34, 36]. As a consequence, a more general model, which admits ideal gas (IG) solutions and considers real gas behavior, is needed for a more precise description of detonation properties in ammonia-based mixtures.

In light of the above motivations, the goals of the present study were (i) to characterize in more detail the detonation sensitivity; (ii) to assess the characteristics length-scale of detonation; and (iii) to study the structure of steady, planar detonation with detailed chemistry for ammonia-based mixtures. A real gas model was used for simulation and the results were compared with ideal gas based solutions to characterize the extent of real gas effect. The manuscript is organized as follows: in the first part, we describe the materials and methods we employed; in the second part, we present the experimental and numerical results we obtained and discuss them in detail; in the last section, we conclude and present future routes of investigation.

2. Materials and methods

2.1. Experimental techniques

Undiluted ammonia-oxygen and ammonia-nitrous oxide mixtures were employed. The mixtures were prepared in a 50 L stainless steel tank using the partial pressure method. All gases were of research grade and obtained from Air Liquide. To ensure composition homogeneity, the mixtures were left to mix through diffusion overnight. The global chemical reactions considered to calculate the stoichiometry of the mixtures were

$$\mathrm{NH_3} + \frac{3}{4}\mathrm{O_2} = \frac{3}{2}\mathrm{H_2O} + \frac{1}{2}\mathrm{N_2}, \tag{1}$$

and

$$\mathrm{NH_3} + \frac{3}{2}\mathrm{N_2O} = \frac{3}{2}\mathrm{H_2O} + 2\mathrm{N_2}, \tag{2}$$

respectively for oxygen and nitrous oxide as the oxidant. The experimental facility employed to study detonation is a 4.6 m long stainless steel tube

with an inner diameter of 78 mm. Before each experiment, the tube was vacuumed to a pressure below 15 Pa. A one-meter long Shchelkin spiral with a blockage ratio of approximately 0.5 was attached at one end of the tube. A flame was spark-ignited in the reactive mixture and the spiral enables the onset of detonation through the deflagration to detonation transition process. To measure the detonation velocity, the opposite end of the tube was equipped with 7 shock detectors located 15 to 30 cm apart from each other. The uncertainty on the velocity of the leading detonation front was 1 % or less. In each experiment, a soot foil was placed at the end of the tube where the shock detectors were located to register the cellular pattern. Soot records were digitized and manually analyzed using the Visilog software. The effect of equivalence ratio and initial pressure on the detonation sensitivity of ammonia-based mixtures were studied within the following ranges: i) for NH_3-O_2, ϕ=0.6-1.5, and P_1=43-100 kPa; ii) for NH_3-N_2O, ϕ=0.3-1.25, and P_1=41-80 kPa. For all experiments, the initial temperature was 295 K. We have performed a total of 25 new experiments in the present work and detailed conditions for each one are listed in table 1.

2.2. Numerical approach

The dynamics of steady planar detonation is described by the Zeldovich, von Neumann, Döering (ZND) theory. Considering a frame of reference attached to the shock, the evolution of the system along the path of a Lagrangian particle (zero-dimensional problem) is described using

$$\eta \frac{dw}{dt} = w\dot{\sigma} \tag{3a}$$

$$\eta \frac{d\rho}{dt} = -\rho\dot{\sigma} \tag{3b}$$

$$\eta \frac{dP}{dt} = -\rho w^2\dot{\sigma} \tag{3c}$$

$$\frac{dy_k}{dt} = \frac{W_k}{\rho}\dot{\omega}_k \tag{3d}$$

where $\eta = 1 - M^2$ is the sonic parameter, w is the velocity, y_k, $\dot{\omega}_k$ and W_k are respectively the mass fraction, source term, and molecular weight of species k. $\dot{\sigma}$ is the non-dimensional energy release rate, or thermicity, whose

EoS-independent expression is given by Schmitt and Butler [37]

$$\dot{\sigma} = \sum_{k=1}^{K} \left(\bar{V}_k - \frac{\beta'}{\rho c_p} \bar{H}_k \right) \frac{\rho}{W_k} \frac{dy_k}{dt}, \quad \text{where } \beta' = \frac{1}{v} \left(\frac{\partial v}{\partial T} \right)_{P,\mathbf{Y}}, \tag{4}$$

where $\bar{V}_k$ and $\bar{H}_k$ are the partial molar volume and the partial molar enthalpy, respectively. $\mathbf{Y}$ is a vector of mass fraction. The partial molar properties are obtained by calculating the partial derivative of the molar properties. More details are provided in [38].

Real gas EoS is needed to close the governing equations. The Peng-Robinson (PR) EoS shows the best consistency with the experimental data of [39] and was thus adopted in this work. Detailed validation is given in the supplementary material. The PR EoS reads

$$P = \frac{RT}{V - b} - \frac{a}{V^2 + 2bV - b^2} \tag{5}$$

where R is the universal gas constant; a and b are parameters to account for the inter-molecular attraction forces and the finite volume of molecules or atoms, respectively. a and b are related to the critical properties (T_c, P_c) and the acentric factor (ω).

$$a_i = 0.45724 \frac{R^2 T_{c,i}^2}{P_{c,i}} \left[1 + f\left(\omega_i\right) \left(1 - T_{r,i}^{0.5} \right) \right]^2 \tag{6a}$$

$$b_i = 0.07780 \frac{R T_{c,i}}{P_{c,i}} \tag{6b}$$

$$f\left(\omega_i\right) = 0.37464 + 1.54226\omega_i - 0.26992\omega_i^2 \tag{6c}$$

Critical properties and acentric factors were obtained as described in Weng et al. [38]. Experimental data are available for stable or metastable species, while for radicals, the Joback's method and the correlations of Stephan et al. [40] were used. For a mixture, the vdW mixing rules are introduced for

a and b in Eq. (7).

$$a = \sum_i \sum_j X_i X_j \left(a_i a_j\right)^{0.5} \left(1 - \overline{k}_{ij}\right) \tag{7a}$$

$$b = \sum_i X_i b_i \tag{7b}$$

where X_i is the mole fraction of species i. $\overline{k}_{ij}$ is the binary interaction coefficient between species i and j. It is determined using experimental binary vapor-liquid equilibrium data [41]. However, the availability of these data is limited and thus $\overline{k}_{ij}$ was treated as zero in the present work, as in most previous works.

The ideal and nonideal thermodynamic functions are connected by departure functions and nonideal EoS [41]. The rate of an elementary reaction in non-ideal system is described by

$$r_i = k_{f,i} \prod_{k=1}^{K} \left(\phi_k \frac{X_k P}{ZRT}\right)^{v'_{k,i}} - k_{r,i} \prod_{k=1}^{K} \left(\phi_k \frac{X_k P}{ZRT}\right)^{v''_{k,i}} \tag{8}$$

where ϕ_k is the fugacity coefficient and Z is the compressibility factor [42]. The forward reaction rate constants ($k_{f,i}$) are explicitly given in the reaction mechanism, while the reverse reaction rate constants are obtained by dividing $k_{f,i}$ by the equilibrium constant.

$$K_{c,i} = \left(\frac{P_0}{ZRT}\right)^{\sum_{k=1}^{K} v_{k,i}} \exp\left(-\frac{\Delta G^0\left(T, P^0\right)}{RT}\right) \tag{9}$$

The ZND model was implemented in the Shock and Detonation Toolbox (SDToolbox) [43] while the real gas model was realized in Cantera [44] by the authors. These tools have been used in previous studies and further details can be found in [38]. During the calculation, the detonation speed is firstly obtained based on CJ theory. Then, the postshock state is solved and used as the initial conditions for integrating Eq. 3. The integration is realized with an ODE solver from SciPy which has adaptive time-step. The relative and absolute tolerances are 10^{-6} and 10^{-12}, respectively. The reaction mechanism of Zhang et al. [17], which is composed of 264 reactions and 38 species, has been adopted for the present study. The mechanism has been validated against a large number of fundamental data for mixtures containing NH_3,

N_2O, NO, NO_2, etc. The experimental data for validation covers a wide pressure range, from ambient pressure to 1 MPa. It is one of the most recent detailed reaction model proposed for describing the combustion of ammonia and it provides accurate predictions of a wide variety of fundamental combustion data. As demonstrated in [17], the performances of the model of Zhang et al. compare rather favorably with respect to other reaction mechanisms from the literature. It is thus well suited for studying detonation in ammonia-based mixtures. The critical properties and acentric factors of all the species are given in supplementary material. The conditions for the numerical calculations are the same as the one used in the experiments, as listed in table 1. In addition, elevated pressure conditions, i.e., 0.1-4.5 MPa were used for stoichiometric NH_3-O_2 and NH_3-N_2O mixtures at 295 K to study the real gas effect.

2.3. Detonation stability parameters

In order to quantify the stability of mixtures we studied, two empirical stability parameters, i.e., the reduced activation energy (θ) [45] and the χ parameter [46] were used. Their respective definitions are

$$\theta = \frac{E_a}{RT_{vN}} = \frac{1}{T_{vN}} \cdot \left(\frac{\ln \tau_{-1} - \ln \tau_{+1}}{1/T_{-1} - 1/T_{+1}} \right) \tag{10a}$$

$$\chi = \frac{T_{vN}}{\Delta_r} \frac{\partial \Delta_i}{\partial T_{vN}} = \theta \frac{\Delta_i}{\Delta_r} = \theta \Delta_i \frac{\dot{\sigma}_{\max}}{w_{CJ}} \tag{10b}$$

where E_a is the global activation energy; T_{vN} is the temperature at von Neumann state; τ, Δ_i, Δ_r and $\dot{\sigma}_{\max}$ are respectively the induction time, induction distance, chemical reaction length, and maximum thermicity of the planar detonation propagating at D_{CJ}; w_{CJ} is the velocity at CJ state in the shock-attached coordinate. Δ_r is approximated as the ratio of w_{CJ} to $\dot{\sigma}_{\max}$. The subscript ± 1 indicates that the parameter was calculated by increasing or decreasing the CJ speed by 1%. The stability of gaseous detonation are related to two aspects, (1) the sensitivity of the induction time to the change of shock strength or postshock temperature, and (2) the ratio of the induction zone length to the chemical reaction length. The former aspect is described by the reduced activation energy while the χ parameter takes both aspects into account. To evaluate the mixture stability, the values of θ and χ are compared to the location of the neutral stability curves obtained from unsteady one-dimensional simulations performed with an irreversible one-step Arrhenius kinetic law [46, 47].

3. Results and discussion

3.1. Experimental results

Figure 1 presents the variation of detonation speed with initial pressure and equivalence ratio in NH_3-O_2 and NH_3-N_2O mixtures. The uncertainty of the measurement is less than 25 m/s or 1%. Since the range of pressure tested is relatively limited, the detonation speeds in both mixture are more sensitive to the equivalence ratio than to the initial pressure. The detonation speed in NH_3-O_2 mixture is much higher than the velocity in NH_3-N_2O mixture, with a difference of 150 - 400 m/s. The experimental results were compared with the CJ speed calculated with IG (D_{CJ}^{IG}) and PR EoS (D_{CJ}^{PR}). The measured speeds are lower than the calculated results over the whole range of conditions considered. The average differences are 2.48% and 3.07% for NH_3-O_2 and NH_3-N_2O respectively. The real gas effect, i.e., the difference of CJ speed calculated with PG and PR EoS, is negligible for the present experimental conditions since the initial pressure is not large enough. In our experiments, either accelerated deflagration or overdriven detonation were observed for leaner mixtures and at lower initial pressures, indicating either that the detonation tube used was too short or that the mixtures were not sensitive enough to obtain self-sustained detonations.

Detonation cell width (λ) measurements were performed in the same range of conditions. The results are presented in Fig. 2 and compared with the prediction obtained using Ng's semi-empirical model [46]. For both mixtures, the characteristics of the cell width variation with initial conditions are similar. When increasing the initial pressure, the cell width decreases according to a power-law. The relation between λ and ϕ is a U-shape curve, with the smallest cell width appearing at $\phi \approx 1$. Although the mixtures with N_2O as oxidizer have much lower detonation speed, they are much more sensitive to detonation than mixtures with O_2. For instance, at $\phi = 1.0$ and $P_1 = 70$ kPa, the cell width in NH_3-O_2 mixture is 3.16 times larger than the one in NH_3-N_2O mixture. The predictions of Ng's model at least qualitatively reproduce the variation of cell width in NH_3-O_2 and NH_3-N_2O mixtures. Quantitatively, Ng's model overpredicts the cell width of both mixtures, but the relative difference is less than 150 %. This is reasonable given that no data for ammonia-based mixture were used to establish Ng's model. It is also noted that the difference tends to increase with initial pressure. Apart from Ng's model, Gavrikov et al. also provided a correlation for

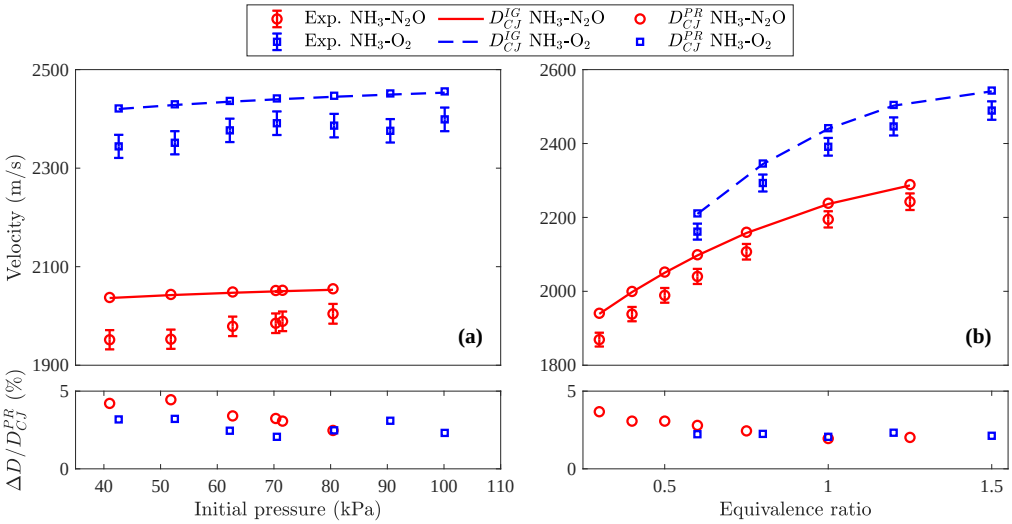

Figure 1: Detonation velocity as a function of (a) initial pressure (P_1) and (b) the equivalence ratio (ϕ) for NH_3-O_2 and NH_3-N_2O mixtures. In (a), $\phi = 0.5$ and 1.0 for mixtures with N_2O and O_2, respectively. In (b), the pressure is 71 kPa. $T_1 = 295$ K.

cell size estimation. However, the results calculated with this latter model is one to two orders of magnitude larger than the experimental data. Details are provided in the supplementary material.

The cell width of NH_3 based mixture was compared with those of other reactive mixtures, including H_2-O_2, CH_4-O_2, C_2H_6-O_2, and C_3H_8-O_2. The results are given in Fig. 3. Compared to the cell width data of hydrogen-, and hydrocarbon-based mixtures, the cell width of ammonia-based mixtures is up to one order of magnitude larger. It indicates that NH_3 is less reactive than other commonly employed fuels. This conclusion is consistent with previous study on the flame speed and ignition delay-time of ammonia based mixtures [20, 17]. All the velocity and cell width results are summarize in table 1.

Two soot foil images are shown in Fig. 4 for stoichiometric NH_3-O_2 and NH_3-N_2O mixtures. The initial pressures are 51.8 kPa and 41 kPa, respectively, while the temperature is 295 K. It was found that the regularity of the cellular structure is low, without clear repeated diamond-shape structure.

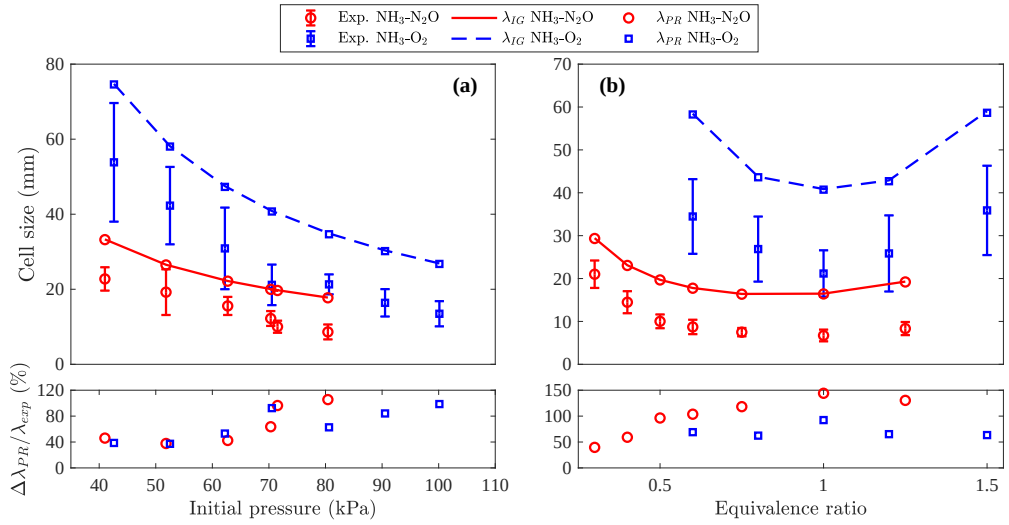

Figure 2: Detonation cell width as a function of (a) P_1 and (b) ϕ for NH_3-O_2 and NH_3-N_2O mixtures. In (a), the equivalence ratios are 1.0 and 0.5 for NH_3-O_2 and NH_3-N_2O mixtures, respectively. In (b), the pressure is 71 kPa. $T_1 = 295$ K.

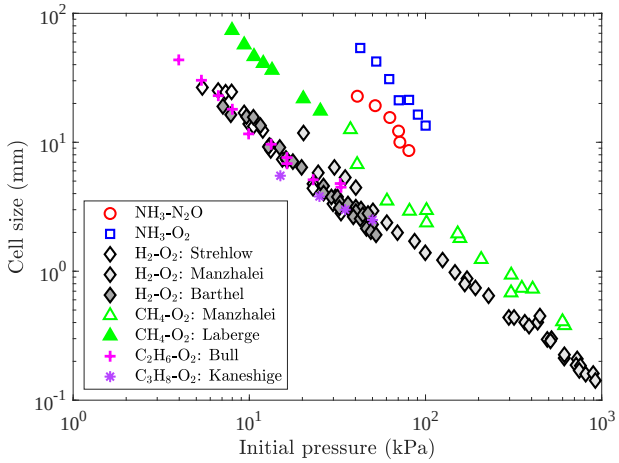

Figure 3: Comparison of the cell width as a function of P_1 for detonation propagating in NH_3-O_2, NH_3-N_2O, H_2-O_2, CH_4-O_2, C_2H_6-O_2, and C_3H_8-O_2 mixtures. ϕ=0.5 for mixtures with NH_3-N_2O and ϕ=1 for all other mixtures; T_1=293-295 K. References: [48, 49, 50, 51, 52, 53].

It indicates that the detonation wave in both mixtures is highly unstable / irregular. The above observation is also supported by the calculation of empirical stability parameters, i.e., the reduced activation energy (θ) and the χ parameter [46]. The stability parameters of ammonia-based mixtures were compared with the corresponding parameters for hydrogen and some hydrocarbon fuels and the neutral stability curves in Fig. 5. In terms of the reduced activation energy, NH_3 based mixtures have similar θ as C_3H_8-$5O_2$-$9N_2$ and H_2-N_2O-$3N_2$. For the χ parameter, NH_3 based mixtures demonstrate similar values than the CH_4+$2O_2$ mixture, which is well known to be highly irregular [54]. In both Fig. 5(a) and 5(b), the points for NH_3-O_2 and NH_3-N_2O all scatter way above the neutral stability curves.

Although the neutral stability curve was calculated from unsteady one-dimensional simulations performed with a one-step irreversible reaction model, these results allow to clearly classify the studied ammonia-based mixtures as highly unstable, which is consistent with the irregular cellular structure in the soot foil experiment, see Fig. 4. Though we only presented the results calculated with PR EoS, it is noted that the real gas effect on the values of θ and χ are minor since the pressure is relatively small, which is consistent with the observations in the calculation of CJ speed (Fig. 1) and cell width (Fig. 2). This minor real gas effect also ensures the applicability of the stability diagrams shown in Fig. 5 which were obtained by considering ideal gas EoS and thermodynamics.

3.2. Real gas effect

In order to investigate in which ranges of initial conditions the real gas effect becomes important, the CJ speed, cell width and stability parameters were calculated over a wide range of initial pressure using EoS-independent solvers for CJ theory and ZND model. The initial temperature was fixed at 295 K.

3.2.1. Detonation velocity and cell width

Figure 6 presents the variations of CJ speed and cell width with initial pressure. Both IG and PR EoS were applied for the calculations. It should be noted that the use of PR EoS for predicting detonation speed has been found to be accurate at initial pressure up to 30 MPa [34]. For all cases, the CJ speed increases with the initial pressure. At ambient pressure, it

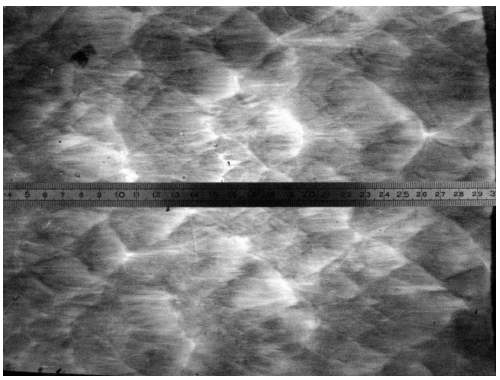

(a) $\phi = 1$; $T_1 = 295$ K; $P_1 = 51.8$ kPa

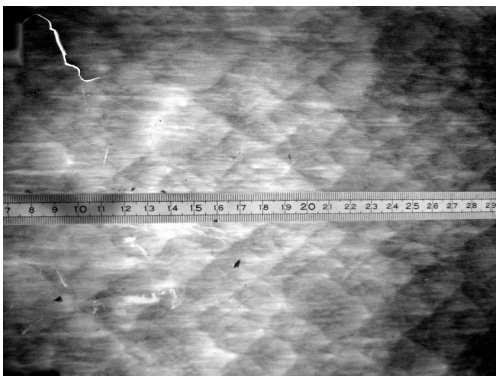

(b) $\phi = 0.5$; $T_1 = 295$ K; $P_1 = 41$ kPa

Figure 4: Examples of soot foils obtained for NH_3-O_2 (a) and NH_3-N_2O (b) mixtures. Propagation from left to right.

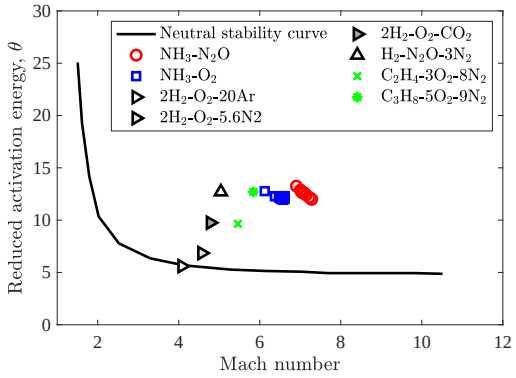

(a) Reduced activation energy

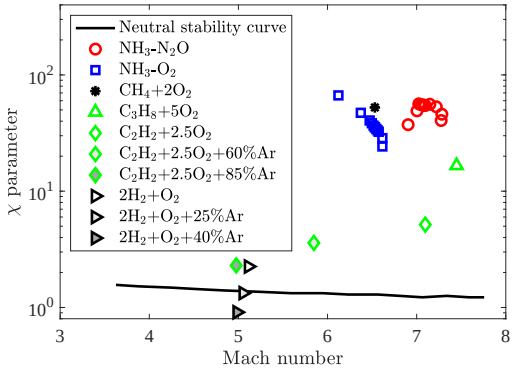

(b) χ parameter

Figure 5: Stability diagram based on (a) reduced activation energy (θ) and (b) χ parameter for a variety of mixtures including NH_3-O_2 and NH_3-N_2O. For NH_3-based mixtures: P_1 = 40-100 kPa, T_1 = 295 K and the Peng-Robinson EoS is used. For other mixtures from the literature: P_1 = 20 kPa, T_1 = 298 K. The neutral stability curves were taken from [46] and [55].

Table 1: Summary of experimental results obtained in [30] and in the present study.

N	X_{NH3}	X_{O2}	X_{N2O}	X_{N2}	ϕ	P_1 (kPa)	T_1 (K)	λ (mm)	$\Delta\lambda$ (mm)	Ref
1	0.571	0.429			1.00	65.9	293	24.5	7.5	Akbar et al.
2	0.513	0.384		0.103	1.00	71.0	293	30.0	12.0	Akbar et al.
3	0.465	0.349		0.186	1.00	73.9	293	36.5	18.5	Akbar et al.
4	0.445	0.333		0.222	1.00	75.9	293	60.0	20.0	Akbar et al.
5	0.426	0.319		0.255	1.00	76.0	293	64.5	14.5	Akbar et al.
6	0.363	0.273		0.364	1.00	81.1	293	101.0	34.0	Akbar et al.
7	0.400		0.600		1.00	55.7	293	11.0	3.0	Akbar et al.
8	0.333		0.500	0.167	1.00	63.8	293	14.0	6.0	Akbar et al.
9	0.286		0.428	0.286	1.00	71.0	293	24.5	8.5	Akbar et al.
10	0.250		0.375	0.375	1.00	76.0	293	45.0	12.0	Akbar et al.
11	0.336	0.034	0.504	0.126	0.88	60.7	293	13.5	4.5	Akbar et al.
12	0.271	0.068	0.407	0.254	0.75	70.9	293	25.5	10.5	Akbar et al.
13	0.205	0.103	0.307	0.385	0.60	86.0	293	46.5	13.5	Akbar et al.
14	0.187	0.112	0.280	0.421	0.56	91.3	293	65.5	33.5	Akbar et al.
15	0.571	0.429			1.00	42.6	295	53.8	15.8	This study
16	0.571	0.429			1.00	52.5	295	42.3	10.3	This study
17	0.571	0.429			1.00	62.2	295	30.9	10.9	This study
18	0.571	0.429			1.00	70.5	295	21.2	5.4	This study
19	0.571	0.429			1.00	80.6	295	21.3	2.7	This study
20	0.571	0.429			1.00	90.5	295	16.4	3.6	This study
21	0.571	0.429			1.00	100.1	295	13.5	3.4	This study
22	0.444	0.556			0.60	71.5	295	34.5	8.7	This study
23	0.516	0.484			0.80	71.5	295	26.9	7.6	This study
24	0.571	0.429			1.00	70.5	295	21.2	5.4	This study
25	0.615	0.385			1.20	71.5	295	25.9	8.9	This study
26	0.667	0.333			1.50	71.5	295	35.9	10.4	This study
27	0.250		0.750		0.50	41.0	295	22.8	3.1	This study
28	0.250		0.750		0.50	51.8	295	19.2	6.1	This study
29	0.250		0.750		0.50	62.7	295	15.6	2.4	This study
30	0.250		0.750		0.50	71.5	295	10.0	1.6	This study
31	0.250		0.750		0.50	70.3	295	12.2	2.0	This study
32	0.250		0.750		0.50	80.4	295	8.6	2.0	This study
33	0.167		0.833		0.30	71.5	295	21.0	3.2	This study
34	0.211		0.789		0.40	71.5	295	14.5	2.6	This study
35	0.250		0.750		0.50	71.5	295	10.0	1.6	This study
36	0.286		0.714		0.60	71.5	295	8.7	1.7	This study
37	0.333		0.667		0.75	71.5	295	7.5	1.0	This study
38	0.400		0.600		1.00	72.0	295	6.7	1.4	This study
39	0.455		0.545		1.25	71.5	295	8.3	1.5	This study

has been shown that the difference of CJ speed calculated with IG and PR EoS is negligible. The real gas effect was observed by continuous increasing the initial pressure. When using IG EoS, the CJ speed asymptotes as the pressure increasing. However, when using the PR EoS for $P_1 > 1$ MPa, the CJ speed of NH_3-O_2 increases linearly with initial pressure, consistent with Schmitt et al.'s finding [34], while that of NH_3-N_2O increases nonlinearly or even exponentially with initial pressure. The relatively difference is about 1% at 1 MPa. At 4.5 MPa, the relative differences are 5.7% and 13.9% for NH_3-O_2 and NH_3-N_2O mixtures, respectively. The exponential variation of the CJ speed was not observed in the work of Schmitt and Butler [34]. We attributed such a behavior to the higher critical temperature of the NH_3-N_2O mixture as compared to the mixtures they have studied. The critical temperature of the NH_3-N_2O mixture is 345.7 K when calculated with the PR EoS. Since it is larger than the initial temperature (295 K) we used, there is a phase change at the CJ state when the initial pressure is increased beyond a certain threshold. The maximum pressure used in the present study is 4.5 MPa. Under such conditions, the mixture is still in gas phase but close to the Widom line in the P-v diagram, as shown in Fig. 7 (a), which is expected to be the boundary of validity of the real gas model we used. To support the above discussion, the initial temperature was raised to 400 K. In this case, the CJ speed increases with the initial pressure without entering the saturation dome and does not show the exponential behaviour, see Fig. 7 (b).

The cell width calculated with Ng's model [46] decreases with initial pressure. At low pressure, the cell width of NH_3-O_2 is larger than the one of NH_3-N_2O, but it decreases more quickly as pressure increases, indicating the overall reaction rate is somehow more sensitive to pressure when O_2 is used as the oxidant. When $P_1 > 600$ kPa, the cell width of NH_3-N_2O becomes larger. Although the real gas effect is much stronger on the CJ speed of NH_3-N_2O mixture than on the one of NH_3-O_2 mixture, the relative difference of cell width for NH_3-N_2O calculated with IG and PR EoS is relatively small in a wide range of initial pressure. The absolute value of relative difference increases exponentially as the initial pressure increases, which is similar to the variation of CJ speed. As for NH_3-O_2 mixture, the relative difference of cell width calculated with IG and PR EoS decreases almost linearly with initial pressure. At 1 MPa, the relative difference is about 4.7%. The inconsistency of real gas effect on CJ speed and cell width can be explained by their dependency on different non-ideal aspects. The calculation of CJ speed

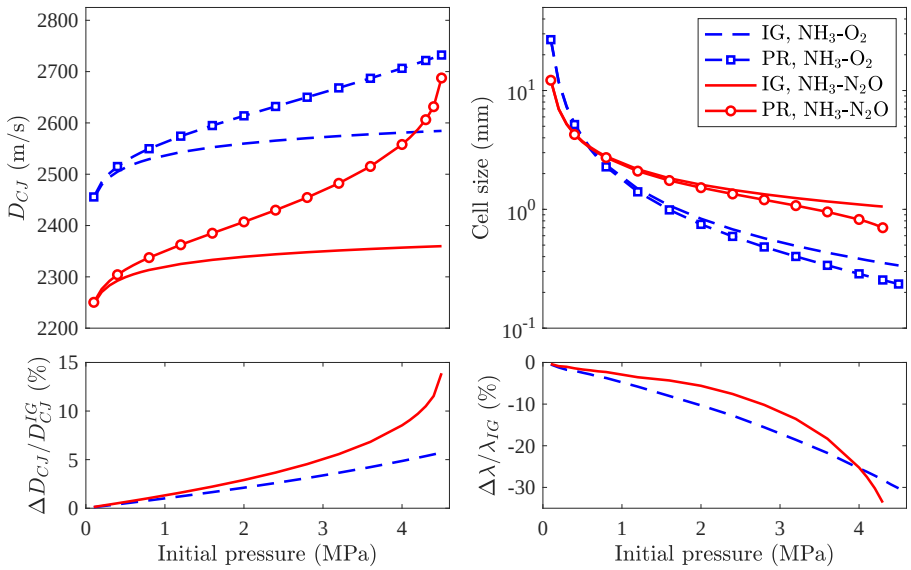

Figure 6: The variation of CJ speed (left) and cell width (right) with initial pressure for stoichiometric NH_3-O_2 and NH_3-N_2O mixture. The cell width is estimated with Ng's method. Both IG EoS (dash line) and PR EoS (solid line) are used for the calculation. T_1 = 295 K.

only depends on the non-ideal EoS and thermodynamic functions. However, the cell width calculated with Ng's model [46] also relies on the reaction kinetics. The inclusion of non-ideal reaction kinetic law, i.e., Eq. 8, is thus part of the overall real gas effect on the cell width calculation. Compared to the IG case, the compressibility factor is added in Eq. 8 to calculate the species concentration while the fugacity coefficient is added for correction related to real gas effect. For an IG, both Z and ϕ_k are equal to 1. The extent of this impact varies with the characteristics of the mixture. A detailed discussion of different non-ideal aspects has been provided in our previous work, see [38]. In the present work, the discussion is limited to the overall impact of RG. For the NH_3-O_2 mixture, the cell width is reduced by as much as 30% at $P_1 > 4.5$ MPa, as a results of these three non-ideal aspects. It is noted that the cell width predicted at high pressure should be interpreted with caution since the model of Ng was developed by considering the ideal gas model. Nevertheless, the qualitative trends are expected to be correct.

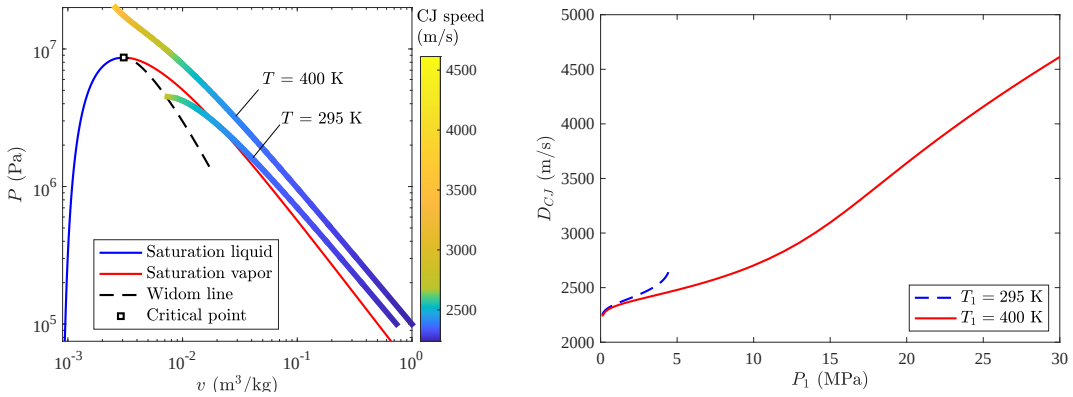

(a) $P - v$ diagram (b) Variation of D_{CJ}^{PR} with initial pressure

Figure 7: The P-v diagram at initial state and CJ speed for the stoichiometric NH_3-N_2O mixture obtained with PR EoS. The CJ speed was calculated with initial conditions of 295 K, 0.1-4.5 MPa and 400 K, 0.1-30 MPa.

3.2.2. Detonation stability

To study the real gas effect on detonation stability, θ and χ were calculated at elevated pressure and are presented in Fig. 8. The reduced activation energy calculated with PR EoS is invariably larger than the one obtained with IG EoS, with a relative difference less than 8%. However, the χ parameter based on PR EoS is lower than the one calculated with the IG EoS, with a maximum difference of 18%. It indicates that calculating these two parameters using the the RG model leads to two opposite conclusions with regard to the detonation stability. When using θ as a criterion, the real gas effect would be expected to destabilize the detonation. In contrast, according to the χ parameter, the detonation would be stabilized by the real gas effect. The two-dimensional cellular detonation simulation by Taileb et al. [35] using Noble-Abel EoS has revealed that the finite molecular volume effect results in a more regular cellular structure. Their observations were explained by the increase of the isentropic coefficient [35] which reads

$$\beta_s = \frac{\rho}{P}\left(\frac{\partial P}{\partial \rho}\right)_s = \gamma\left(\frac{\partial \ln P}{\partial \ln \rho}\right)_T, \tag{11}$$

where s is the entropy, γ is the heat capacity ratio, i.e., c_P/c_v. For IG EoS, the isentropic coefficient is simply equal to the heat capacity ratio. The study of Mach [56] based on IG EoS has revealed that decreasing β_s leads to inert shock front bifurcation and thus enhances the irregularity of the detonation.

However, for non-ideal EoS, not only γ is affected by the real gas effect. In addition, the partial derivative term in Eq. (11) is not unity. The variation of β_s in the same range of initial pressure is given in Fig. 9. The isentropic coefficient was calculated at the von Neumann state. It was found that β_s of both NH_3-O_2 and NH_3-N_2O mixtures based on PR EoS increases with the initial pressure. In terms of detonation stability, the variation of β_s would thus lead to the same conclusion as the one drawn from the analysis of the evloution of the χ parameter with pressure. The parameter β_s is nearly constant when calculated with the IG EoS. The reason is that β_s of an IG depends on temperature but not on pressure. Since the CJ speed is not sensitive to initial pressure, see Fig. 6, the postshock temperature is also insensitive to initial pressure, and thus β_s has similar behavior. The results imply that at elevated pressure, (1) the real gas model should be used to include the pressure effect; (2) the χ parameter is a more appropriate parameter to judge the stability of detonation wave. The latter conclusion seems reasonable when recalling that the χ parameter considers more aspects relevant to detonation instability as discussed in section 2.3. Nevertheless, the stability of detonation at elevated pressure remains a rarely studied topic. Although Taileb [35] performed the first two-dimensional simulation of detonation based on the real gas model, some non-ideal aspects, like the inter-molecular attraction force, were neglected. We present in the supplementary material additional calculations performed with the NA EoS. These show that the effect of the inter-molecular attraction force is not negligible, although the overall qualitative behavior is not affected by it. The increased detonation stability when increasing pressure and the mechanism behind remain to be further understood.

3.3. Steady structure and thermo-chemical dynamics

In this section, detailed thermo-chemical analyses were performed to characterize the reaction zone structure and dominant reactions of ZND detonation in NH_3-O_2 and NH_3-N_2O mixtures. Two values of initial pressure were considered, i.e., 70 kPa and 4 MPa. The former one falls in the range of experimental conditions and was studied with the IG EoS. The latter one was selected to investigate the real gas effect and calculation for this condition was accomplished with the PR EoS. The equivalence ratio was 1.0 and the initial temperature was 295 K.

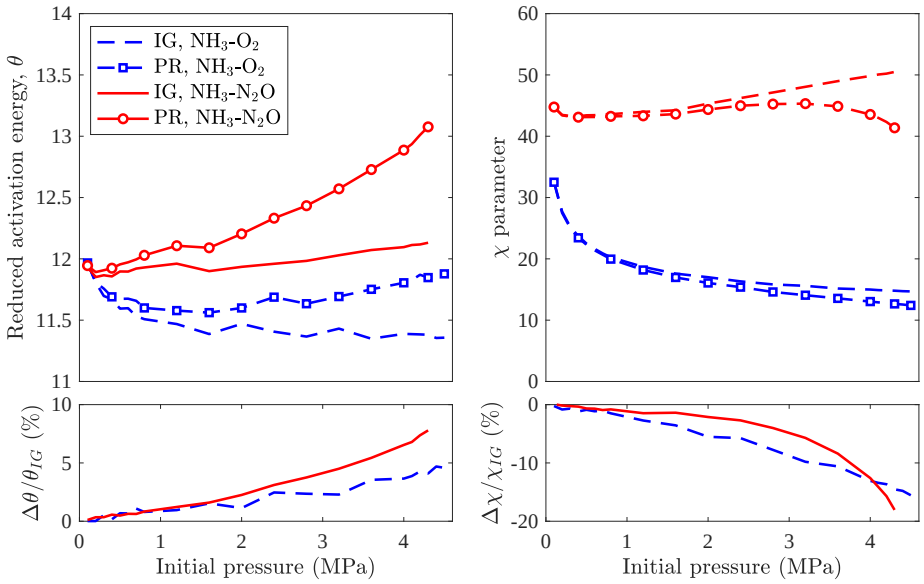

Figure 8: Variation of stability parameters (θ and χ) with initial pressure for stoichiometric NH_3-O_2 and NH_3-N_2O mixtures. Both IG EoS (dash line) and PR EoS (solid line) are used for the calculation. $T_1 = 295$ K.

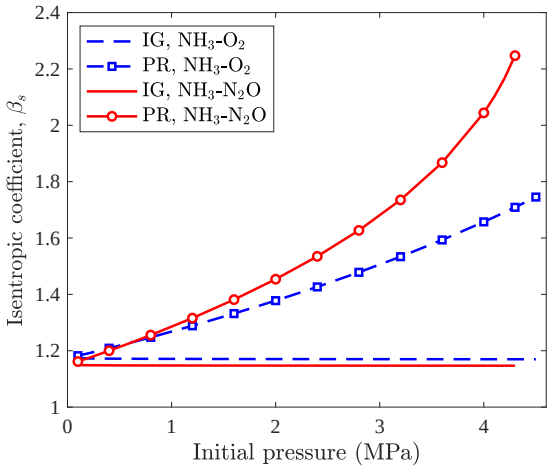

Figure 9: Variation of isentropic coefficient (β_s) with initial pressure for stoichiometric NH_3-O_2 and NH_3-N_2O mixture. Both IG EoS (dash line) and PR EoS (solid line) are used for the calculation. $T_1 = 295$ K.

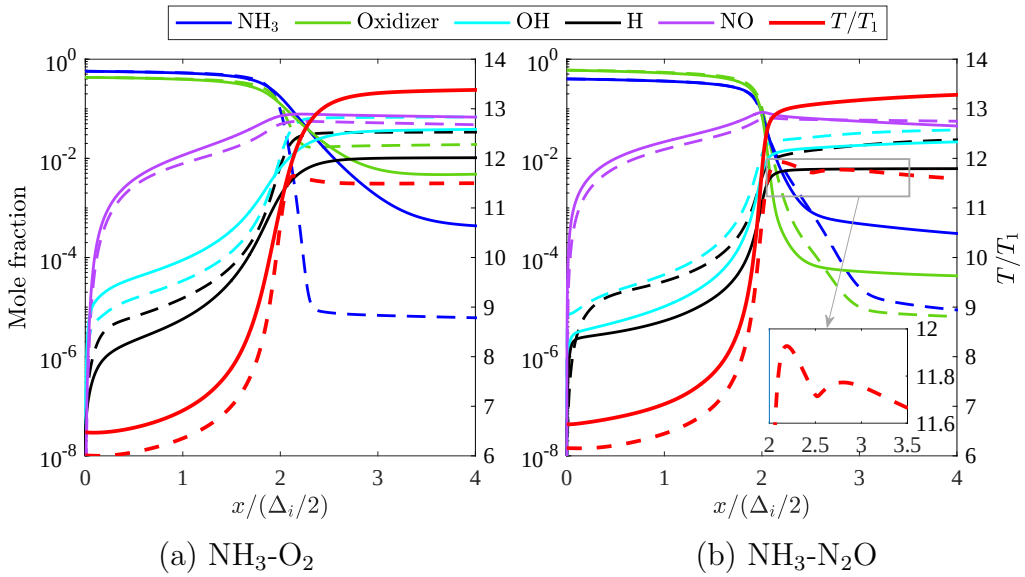

(a) NH_3-O_2 (b) NH_3-N_2O

Figure 10: Mole fraction and temperature profiles of ZND detonation in stoichiometric (a) NH_3-O_2 and (b) NH_3-N_2O mixtures at 70 kPa (dash line) and 4 MPa (solid line). The IG EoS was used for low pressure while the PR EoS was used for elevated pressure condition. $T_1 = 295$ K.

3.3.1. Structure of ZND detonation

Figure 10 presents selected mole fraction and temperature profiles. The distance and temperature were non-dimensionalized with half of the induction distance and the initial temperature, respectively. It is recalled that the induction distance decreases with initial pressure. In stoichiometric NH_3-O_2 mixture, Δ_i are 1.28×10^{-3} m (70 kPa) and 7.50×10^{-6} m (4 MPa), respectively, while the values for stoichiometric NH_3-N_2O are 5.04×10^{-4} m (70 kPa) and 2.47×10^{-5} m (4 MPa), respectively. At low pressure, NH_3-N_2O has shorter induction distance while at elevated pressure, the mixture has larger induction distance. This observation is consistent with the evolution of cell width with initial pressure given in Fig. 6.

The mole fractions of NH_3 and oxidizer are nearly constant in the induction zone and then quickly decrease as the chain reactions proceed. When using the dimensionless distance, the rate of decrease of the mole fraction of NH_3 is similar at low and high pressure for NH_3-N_2O mixture. However, in

NH_3-O_2 mixture, the mole fraction of NH_3 decreases much faster at 70 kPa. A similar behavior is observed for the variation of the oxidizer mole fraction. As for the mole fraction profiles of the radicals, H and NH_2 radicals are firstly generated through R160: $NH_3 + M = H + NH_2 + M$ after the shock compression, followed by a sharp increase of OH radical and NO radical. In the induction zone, the NO radical dominates other radicals as the reaction proceeds. Around the end of the induction zone, the amount of OH radical increases quickly and finally surpass the amount of NO.

3.3.2. Pathological behavior

At low pressure, the temperature profiles of both NH_3-N_2O and NH_3-O_2 mixtures show a pathological detonation behaviour [57]. The steady pathological detonation refers to steady detonation with velocity larger than the CJ speed. Such a behavior has been identified for H_2-Cl_2 mixtures both in experiment and simulation by Dionne et al. [58]. Lee [27] and Higgins [57] provide comprehensive discussion on the characteristics of steady pathological detonation. The cause for such phenomenon is that CJ theory assumes the CJ criterion, i.e., the local flow velocity reaches Mach 1 with respect to the shock front, is satisfied as the chemical reactions are complete and the system has reached thermodynamic equilibrium. With this assumption, the Rayleigh line is tangent to the equilibrium Hugoniot curve. However, it is possible that the CJ criteria is satisfied before the chemical reactions have evolved to completion. In this case, the Rayleigh line is tangent to an intermediate Hugoniot curve. The internal structure of the reaction zone should be considered to obtain the steady detonation speed, which is larger than the CJ speed.

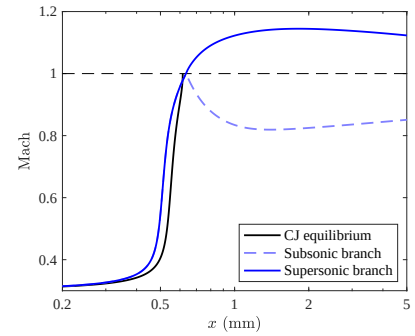

(a) Mach number

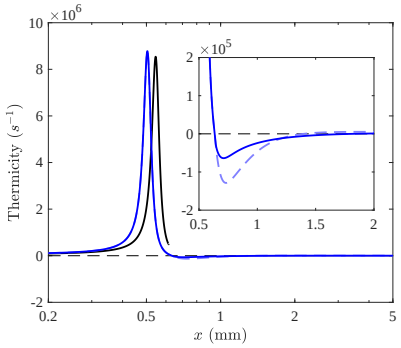

(b) Thermicity

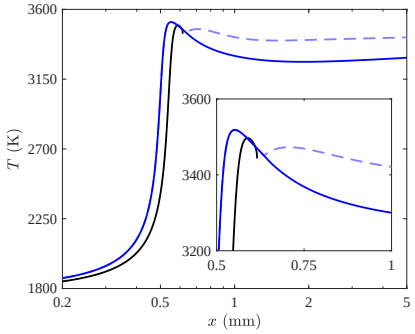

(c) Temperature

Figure 11: CJ equilibrium and eigenvalue (i.e. subsonic and supersonic branches) solutions for pathological detonation in stoichiometric NH_3-N_2O mixture. $P_1 = 70$ kPa. $T_1 = 295$ K.

From the perspective of heat release, the pathological detonation is characterized by an exothermic process immediately followed by an endothermic process [57]. The CJ speed is calculated by considering the total heat release which is less than the amount of heat released solely by the exothermic process. In other words, the CJ speed calculated by considering solely the heat release of the exothermic process should be higher than the former one. As a result, solving the ZND structure with the CJ speed as the shock speed (i.e. the CJ equilibrium solution) demonstrates a singularity issue. When the initial pressure is 70 kPa, the CJ speed needs to be increased by 0.475% (NH_3-N_2O) and 0.05% (NH_3-O_2) in order to avoid the singularity issue near the sonic state, i.e. eigenvalue solutions. Figure 11 presents the Mach number, thermicity, temperature and pressure profiles obtained by considering the CJ equilibrium and eigenvalue solutions. The CJ equilibrium solution was obtained by using the CJ speed of the shock speed and solve the ZND equations. At sonic state, $\eta = 0$ but $\sigma \neq 0$, which results in a singularity, see Eq. 3 and Fig. 11(a). The CJ eigenvalue solution was found by searching the detonation speed that allows $\dot{\sigma} \to 0$ when $M \to 1.0$. This condition enables the governing equations being satisfied at the sonic state. The eigenvalue solution consists of a supersonic branch and a subsonic branch, as shown in Fig. 11(a). In the shock-attached coordinate, the flow continues accelerating smoothly after the sonic state in the supersonic branch, while the flow velocity drops in the subsonic branch. The exothermic and endothermic processes are seen in Fig. 11(b) as thermicity changing from positive to negative around the sonic point. The temperature profile of the supersonic solution, presented in Fig. 11(c) demonstrates a single peak and then asymptotes to its final value. The temperature profile of the subsonic solution is more complex and exhibits a characteristic double peak of temperature. The temperature reaches the first peak, then slightly decreases and increases again to reach the second peak. Finally, it decreases asymptotically to the final state.

The present results are qualitatively consistent with the solutions of [57] using a two-step reaction model and a detailed reaction model for H_2-Cl_2 mixtures. At elevated pressure, the pathological detonation behavior disappears, indicating the endothermic process becomes less pronounced compared to the exothermic process. Such a behavior is also consistent with previous results on pathological detonation [58]. Recognizing that a much more pronounced pathological behavior has been observed for H_2-Cl_2 mixtures, we would like to emphasize that it is possible that the pathological behavior in NH_3-N_2O

mixtures could be more dramatic at lower initial pressure and for a different equivalence ratio. Such an detail investigation is kept for a future study.

3.3.3. Thermo-chemical analyses for ZND detonation

To determine the dominant reactions responsible for heat production and consumption, the heat release by each reaction was analyzed and presented in Fig. 12. In stoichiometric NH_3-O_2 mixture, dominant reactions in releasing heat are similar for low- and elevated-pressure conditions. The reactions R162 (NH_3 + OH = H_2O + NH_2) and R175 (NNH + O_2 = HO_2 + N_2) are equally important in term of heat release. The reaction between NH_2 radicals (R88) is the third most important for heat release. Two pressure-dependent reactions, i.e., R78 (N_2H_2 + M = H + NNH + M) and R29 (H_2O_2 (+M) = 2OH (+M)) absorb the largest amount of heat. In addition, R78 provides NNH radical for R175, while R29 provides OH radical for R162. Fig. 12(a) also shows that the relative amount of heat absorbed by R1 (H + O_2 = O + OH) decrease significantly as pressure increases. In contrast, R29 becomes much more important at high pressure due to its pressure dependence. The other reason is that the HO_2 radical becomes more reactive at high pressure and R29 acts as an important chain-branching reaction, which is similar to the explosion mechanism at high pressure in H_2/O_2 mixture. In NH_3-N_2O mixture, although R78 and R162 are still important, reactions that involve N_2O play more important roles in heat release or absorption. The chain-propagation reaction R206 (H + N_2O = N_2 + OH) releases the largest amount of heat, while reaction R205 (N_2O (+M) = N_2 + O (+M)) absorbs the largest amount of heat. Without O_2 as the oxidizer, the reaction between NNH and O_2 is not dominant, and NNH, produced by R78, is converted to N_2 by reacting with NO (R169) and NH_2 (R171).

Aside from investigating the dominant reactions governing heat release, a sensitivity study was performed to study the key reactions influencing the characteristic length-scale, i.e., the induction distance, of detonation. The sensitivity coefficient of the ith reaction (S_i) was calculated by perturbing each reaction rate constant by 1%, i.e.

$$S_i = \frac{k_{f,i}}{\Delta_i}\frac{\partial \Delta_i}{\partial k_{f,i}} \approx 100\frac{\Delta_i^+ - \Delta_i}{\Delta_i}, \tag{12}$$

where $k_{f,i}$ is the forward reaction rate constant of the i^{th} reaction. The superscripts + denotes the perturbed value and the nominal value respectively.

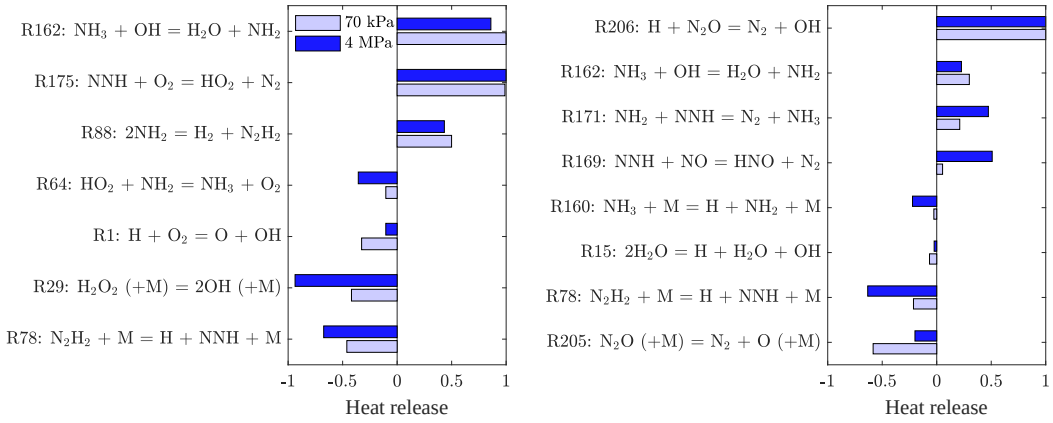

(a) NH_3-O_2 (b) NH_3-N_2O

Figure 12: Heat release by different reactions for ZND detonation in stoichiometric (a) NH_3-O_2 and (b) NH_3-N_2O mixture at 70 kPa (dash line) and 4 MPa (solid line). The IG EoS was used for low pressure while the PR EoS was used for elevated pressure condition. $T_1 = 295$ K.

The results, presented in Fig. 13, were normalized with the maximum sensitivity coefficient for each condition.

In stoichiometric NH_3-O_2 mixture, the induction distance is most sensitive to R63 ($HO_2 + NH_2 = H_2NO + OH$). By performing jet-stirred reactor experiments at atmospheric pressure and intermediate temperature, Zhang et al. [17] have found that R63 is an important intermediate reaction to convert HO_2 to OH radical. Rate of progress (RoP) analysis also shows that R63 is also one of the dominant reactions in supplying OH under detonation conditions. Details of the RoP analysis for OH is provided in the supplementary material. At 70 kPa, R1 also affects the induction distance, but its effect diminishes at elevated pressure. At the same time, R1 is the major reaction supplying OH at low pressure. In stoichiometric NH_3-N_2O mixture, the induction distance is also sensitive to the main reaction producing OH radical, i.e., R207. In addition, Fig. 13(b) shows that the induction distance of NH_3-N_2O mixture is sensitive to reactions that involve N_2O. Reaction R205: N_2O (+M) = N_2 + O (+M) is the most sensitive one and enables to initiate the overall reaction by releasing O radical. Reaction R207 provides another channel to react with N_2O, and is the second most sensitive reaction.

The results obtained for the NH_3-N_2O mixture are consistent with previous results obtained for H_2-N_2O mixtures under auto-ignition and flame conditions, see [59, 60, 61].

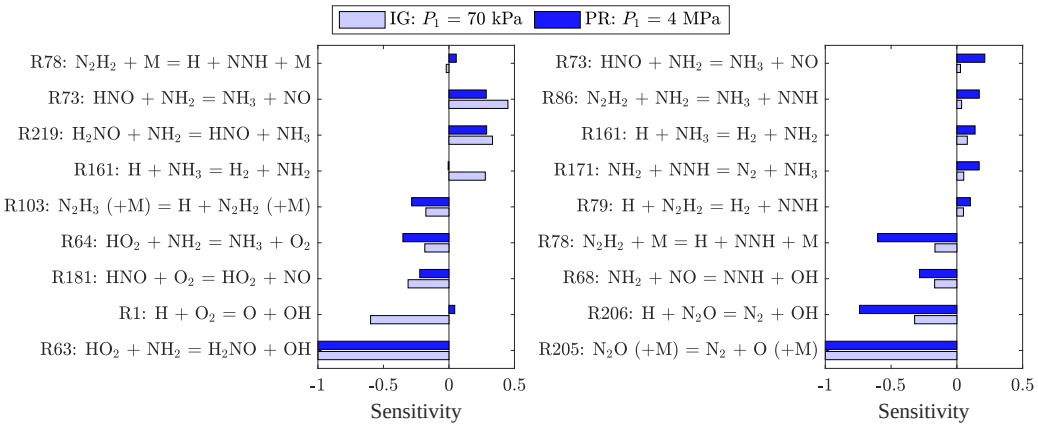

(a) NH_3-O_2 (b) NH_3-N_2O

Figure 13: Sensitivity of induction distance (Δ_i) to the reaction rate constant for ZND detonation in stoichiometric (a) NH_3-O_2 and (b) NH_3-N_2O mixtures. Only the three reactions with the highest or lowest (negative) S_i are presented for each case. The IG EoS was used for low pressure condition while the PR EoS was used for elevated pressure condition. T_1 = 295 K.

The heat release and sensitivity analysis given above were coupled with RoP analysis to study the reaction pathways for NH_3-O_2 and NH_3-N_2O mixtures, as shown in Fig. 14 and 15. In the two mixtures, OH is the dominant radical to react with NH_3 via chain-propagation reaction (R162) which is also the major exothermic reaction. The NH_2 produced in R162 can react with itself to form N_2H_2. This intermediate species is further converted to NNH and N_2. In NH_3-O_2 mixture (Fig. 14), the consumption of NH_2 also takes place via reaction with HO_2, which is the most sensitive reaction for the induction zone length of the ZND detonation. Following this reaction, the product H_2NO is further converted to NH_3 and H_2O_2, which is one of the key sources for producing OH radical. In NH_3-N_2O mixture (Fig. 15), the presence of N_2O provides another pathway for converting NH_2 to N_2H_2. At the same time, N_2O reacts with H radical (R207) and a collision partner (R205). These two reactions govern the heat release process, provide OH and

O radicals, and sensitively affect the induction distance. By comparing the contribution of each reaction, the reaction pathways remain similar at low- and high-pressure conditions, regardless of the gas model employed, i.e., ideal or real gas. The major difference is that the pressure-dependent reactions are enhanced at elevated conditions.

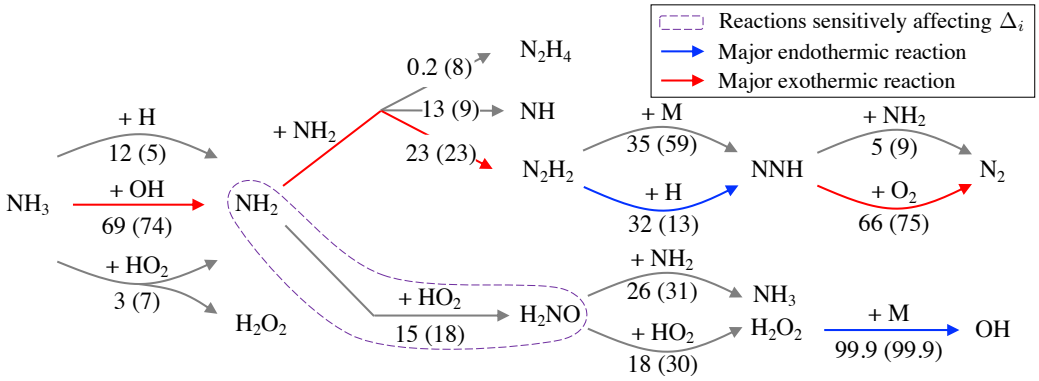

Figure 14: The reaction pathways based on the RoP analysis for stoichiometric NH_3-O_2 mixture. Numbers below each arrow refer to the percentage of species consumed by the reaction at 70 kPa and 4 MPa (in parenthesis). The IG EoS was used for low pressure while the PR EoS was used for elevated pressure condition. $T_1 = 295$ K.

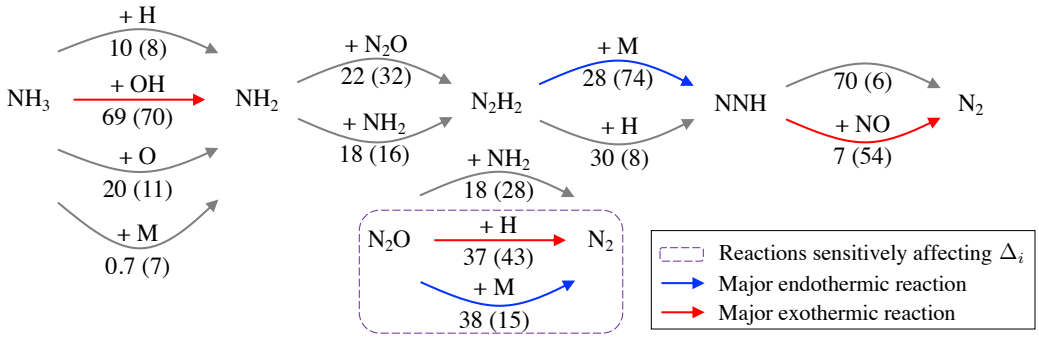

Figure 15: The reaction pathways based on the RoP analysis for stoichiometric NH_3-N_2O mixture. Numbers below each arrow refer to the percentage of species consumed by the reaction at 70 kPa and 4 MPa (in parenthesis). The IG EoS was used for low pressure while the PR EoS was used for elevated pressure condition. $T_1 = 295$ K.

Although the application and fundamental studies on ammonia have received growing attention in recent years, there are still lacks concerning studies on detonation. According to our literature review, several DDT studies were done but fundamental data, like cell width, critical tube diameter, etc are not detailed enough or not available. The present study provides experimental measurement of detonation speed and cell width below ambient pressure and at 295 K. Pathological detonation behaviour was observed via simulation using the ZND model. Evidences of such a phenomenon from experiment are not available and this could be one of the topics for future study. By using a real gas model, the detonation properties, including stability and length scale were estimated for elevated pressure condition, which should be more relevant to the conditions of industrial application, like gas turbine, or internal combustion engine. These results provide a fundamental understanding on the detonation behavior of ammonia-based mixtures at elevated pressure. However, they should receive further validation in future experimental investigations.

4. Conclusions

In the present study, detonation in NH_3-O_2 and NH_3-N_2O mixtures was investigated experimentally and numerically. In experiments below ambient pressure, mixtures with N_2O as an oxidizer have smaller induction distance and cell width and thus, are more sensitive to detonation than mixtures with oxygen as oxidizer. At elevated pressure, up to 4.5 MPa, the real gas effects were considered and the conclusion is the opposite. Overall, detonation in ammonia-based mixtures are highly unstable and do not demonstrate a high sensitivity since it was required to use undiluted mixtures to initiate detonation in our laboratory-scale experimental facility. The stability of the detonation is enhanced at elevated pressure owing to a higher isentropic coefficient. Detailed thermo-chemical studies show a pathological detonation behaviour at low pressure in ammonia-based mixtures. The heat release is governed by $NH_3 + OH = NH_2 + H_2O$ in NH_3-O_2 but $H + N_2O = N_2 + OH$ becomes dominant in NH_3-N_2O mixture. The hydroxyl radical, OH, is one of the dominant radicals, which is supplied by $H + O_2 = O + OH$ (low pressure) and H_2O_2 (+M) = 2OH (+M) (elevated pressure) in NH_3-O_2 mixture and by $H + N_2O = N_2 + OH$ in NH_3-N_2O mixture. The induction distance is sensitive to reactions involved in the production/consumption of OH radical in both mixtures. In NH_3-N_2O mixture, the induction distance

is also sensitive to reactions involving the oxidizer, N_2O.

Acknowledgements

The experimental work performed at ICARE-CNRS Orléans was partially supported by the French "Ministère de l'Éducation Nationale, de l'Enseignement Supérieur et de la Recherche" (ATER funding) and by Centre National de la Recherche Scientifique. RM is grateful to Professor Claude-Étienne Paillard for useful discussion during the experiments.

References

[1] O. Elishav, B. Mosevitzky Lis, E. Miller, D. Arent, A. Valera-Medina, A. Grinberg Dana, G. Shter, G. Grader, Progress and prospective of nitrogen-based alternative fuels, Chemical Review 120 (12) (2020) 5352–5436.

[2] H. Kobayashi, A. Hayakawa, K. Kunkuma, A. Somarathne, E. Okafor, Science and technology of ammonia combustion, Proceedings of the Combustion Institute 37 (2019) 109–133.

[3] Q. Liu, X. Chen, J. Huang, Y. Shen, Y. Zhang, Z. Liu, The characteristics of flame propagation in ammonia/oxygen mixtures, Journal of Hazardous Materials 363 (2019) 187–196.

[4] X. Han, M. Lavadera, A. Konnov, An experimental and kinetic modeling study on the laminar burning velocity of NH_3+N_2O+air flames, Combustion and Flame 228 (2021) 13–28.

[5] K. Shrestha, C. Lhuillier, A. Alves Barbosa, P. Brequigny, F. Contino, C. Mounaim-Rousselle, L. Seidel, F. Mauss, An experimental and modeling study of ammonia with enriched oxygen content and ammonia/hydrogen laminar flame speed at elevated pressure and temperature, Proceedings of the Combustion Institute 38 (2021) 2163–2174.

[6] O. Mathieu, E. Petersen, Experimental and modeling study on the high-temperature oxidation of ammonia and related NOx chemistry, Combustion and Flame 162 (3) (2015) 554–570.

[7] B. Shu, S. Vallabhuni, X. He, G. Issayev, K. Moshammer, A. Farooq, R. Fernandes, A shock tube and modeling study on the autoignition properties of ammonia at intermediate temperatures, Proceedings of the Combustion Institute 37 (2019) 205–211.

[8] X. He, B. Shu, D. Nascimento, K. Moshammer, M. Costa, R. Fernandes, Auto-ignition kinetics of ammonia and ammonia/hydrogen mixtures at intermediate temperatures and high pressures, Combustion and Flame 206 (2019) 189–200.

[9] L. Daia, S. Gersen, P. Glarborg, H. Levinsky, A. Mokhov, Experimental and numerical analysis of the autoignition behavior of NH_3 and NH_3/H_2 mixtures at high pressure, Combustion and Flame 215 (2020) 134–144.

[10] H. Nakamura, S. Hasegawa, T. Tezuka, Kinetic modeling of ammonia/air weak flames in a micro flow reactor with a controlled temperature profile, Combustion and Flame 185 (2017) 16–27.

[11] A. Stagni, C. Cavallotti, S. Arunthanayothin, Y. Song, O. Herbinet, F. Battin-Leclerc, T. Faravelli, An experimental, theoretical and kinetic-modeling study of the gas-phase oxidation of ammonia, Reaction Chemistry & Engineering 5 (2020) 696–711.

[12] M. Abian, M. Benes, A. de Goni, B. Munez, M. Alzueta, Study of the oxidation of ammonia in a flow reactor. experiments and kinetic modeling simulation, Fuel 300 (2021) 120979.

[13] M. Benes, G. Pozo, M. Abian, A. Millera, R. Bilbao, M. Alzueta, Experimental study of the pyrolysis of NH_3 under flow reactor conditions, Energy & Fuels 35 (2021) 7193–7200.

[14] L. Kawka, G. Juhasz, M. Papp, T. Nagy, I. Zsely, T. Turanyi, Comparison of detailed reaction mechanisms for homogeneous ammonia combustion, Zeitschrift fur Physikalische Chemie 234 (7-9) (2020) 1329–1357.

[15] H. Xiao, A. Valera-Medina, Chemical kinetic mechanism study on premixed combustion of ammonia/hydrogen fuels for gas turbine use, Journal of Engineering for Gas Turbines and Power 139 (2017) # 081504.

[16] K. Shrestha, L. Seidel, T. Zeuch, F. Mauss, Detailed kinetic mechanism for the oxidation of ammonia including the formation and reduction of nitrogen oxides, Energy & Fuels 32 (10) (2018) 10202–10217.

[17] X. Zhang, S. Moosakutty, R. Rajan, M. Younes, S. Sarathy, Combustion chemistry of ammonia/hydrogen mixtures: Jet-stirred reactor measurements and comprehensive kinetic modeling, Combustion and Flame 234 (2021) # 111653.

[18] A. Bertolino, M. Furst, A. Stagni, A. Frassoldati, M. Pelucchi, C. Cavallotti, T. Faravelli, A. Parente, An evolutionary, data-driven approach for mechanism optimization: theory and application to ammonia combustion, Combustion and Flame 229 (2021) # 111366.

[19] P. Berwal, S. Kumar, B. Khandelwal, A comprehensive review on synthesis, chemical kinetics, and practical application of ammonia as future fuel for combustion, Journal of the Energy Institute 99 (2021) 273–298.

[20] A. Valera-Medina, H. Xiao, M. Owen-Jones, W. David, P. Bowen, Ammonia for power, Progress in Energy and Combustion Science 69 (2018) 63–102.

[21] G. Thomas, Flame acceleration and the development of detonation in fuel-oxygen mixtures at elevated temperatures and pressures, Journal of Hazardous Materials 163 (2009) 783–794.

[22] G. Thomas, G. Oakley, R. Bambrey, An experimental study of flame acceleration and deflagration to detonation transition in representative process piping, Process Safety and Environmental Protection 88 (2010) 75–90.

[23] Q. Jing, J. Huang, Q. Liu, D. Wang, X. Chen, Z. Wang, C. Liu, The flame propagation characteristics and detonation parameters of ammonia/oxygen in a large-scale horizontal tube: As a carbon-free fuel and hydrogen-energy carrier, International Journal of Hydrogen Energy 46 (2021) 19158–19170.

[24] M. Kaneshige, J. E. Shepherd, Detonation database, Tech. Rep. FM97-8, GALCIT (1997).

[25] Q. Xiao, C. Weng, Unified dynamics of hydrogen-oxygen-diluent detonations in narrow confinements, Fuel 334 (2023) # 126661.

[26] B. Zhang, H. D. Ng, R. Mével, J. H. S. Lee, Critical energy for direct initiation of spherical detonations in $H_2/N_2O/Ar$ mixtures, International Journal of Hydrogen Energy 36 (2011) 5707–5716.

[27] J. H. S. Lee, The Detonation Phenomenon, Cambridge University Press, 2008.

[28] S. Gallier, F. Le Palud, F. Pintgen, R. Mével, J. Shepherd, Detonation wave diffraction in H_2-O_2-Ar mixtures, Proceedings of the Combustion Institute 36 (2017) 2781–2789.

[29] M. Radulescu, R. Mével, Q. Xiao, S. Gallier, On the self-similarity of diffracting gaseous detonations and the critical channel width problem, Physics of Fluids 33 (2021) 066106.

[30] R. Akbar, M. Kaneshige, E. Schultz, J. Shepherd, Detonations in H_2-N_2O-CH_4-NH_3-O_2-N_2 mixtures, Tech. Rep. FM-97-3, Explosion Dynamics Laboratory, California Institute of Technology (1997).

[31] P. Atkins, J. de Paula, Physical Chemistry, Eighth Edition, 8th Edition, Oxford University Press, 2016.

[32] R. Gealer, S. Churchill, Detonation characteristics of hydrogen-oxygen mixtures at high initial pressures, AIChE Journal 6 (3) (1960) 501–505.

[33] P. Bauer, Contribution a l'étude de la détonation de mélanges explosifs gazeux à pression initiale élevée, Ph.D. thesis, Université de Poitiers (1985).

[34] R. Schmitt, P. Butler, Detonation properties of gases at elevated initial pressures, Combustion Science and Technology 106 (1995) 167–191.

[35] S. Taileb, J. Melguizo-Gavilanes, A. Chinnayya, Influence of the equation of state on the cellular structure of gaseous detonations, Physics of Fluids 33 (2021) #036105.

[36] R. Schmitt, P. Butler, Detonation wave structure of gases at elevated initial pressures, Combustion Science and Technology 107 (1995) 355–385.

[37] R. Schmitt, P. Butler, Chemkin real gas: A fortran package for analysis of their properties and chemical kinetics in nonideal systems, Tech. rep., The University of Iowa (1994).

[38] Z. Weng, R. Mevel, Real gas effect on steady planar detonation and uncertainty quantification, Combustion and Flame 245 (2022) # 112318.

[39] L. Haar, J. S. Gallagher, Thermodynamic properties of ammonia, Journal of Physical and Chemical Reference Data 7 (3) (1978) 635–792.

[40] S. Stephan, M. Thol, J. Vrabec, H. Hasse, Thermophysical properties of the Lennard-Jones fluid: database and data assessment, Journal of Chemical Information and Modeling 59 (10) (2019) 4248–4265.

[41] B. Poling, J. Prausnitz, J. O'Connell, The properties of gases and liquids, 5th Edition, McGraw-Hill, 2001.

[42] W. Tang, K. Brezinsky, Chemical kinetic simulations behind reflected shock waves, International Journal of Chemical Kinetics 38 (2005) 75–97.

[43] S. Browne, J. Ziegler, N. Bitter, B. Schmidt, J. Lawson, J. Shepherd, Numerical tools for shock and detonation wave modeling, Tech. rep., Explosion Dynamics Laboratory, Graduate Aerospace Labortories, California Institute of Technology, Pasadena, CA USA 91125 (2021).

[44] D. G. Goodwin, H. K. Moffat, I. Schoegl, R. L. Speth, B. W. Weber, Cantera: An object-oriented software toolkit for chemical kinetics, thermodynamics, and transport processes, https://www.cantera.org, version 2.4.0 (2018).

[45] E. Schultz, J. Shepherd, Validation of detailed reaction mechanisms for detonation simulation, Tech. Rep. FM-99-5, GALCIT (2000).

[46] H. D. Ng, The effect of chemical reaction kinetics on the structure of gaseous detonations, Ph.D. thesis, McGill University (2005).

[47] C. A. Eckett, J. J. Quirk, J. E. Shepherd, The role of unsteadiness in direct initiation of gaseous detonations., Journal of Fluid Mechanics 421 (2000) 147–183.

[48] R. Strehlow, R. Maurer, S. Rajan, Transverse waves in detonations: II. structure and spacing in the H_2-O_2, C_2H_2-O_2, C_2H_4-O_2, and CH_4-O_2 systems, AIAA Journal 7 (3) (1969) 492–496.

[49] V. Manzhalei, V. Mitrofanov, V. Subbotin, Measurement of inhomogeneities of a detonation front in gas mixtures at elevated pressures, Combustion, Explosion, and Shock Waves 10 (1) (1974) 89–95.

[50] H. Barthel, Predicted spacings in hydrogen-oxygen-argon detonations, Physics of Fluids 17 (8) (1974) 1547–1553.

[51] S. Laberge, R. Knystautas, J. Lee, Propagation and extinction of detonation waves in tube bundles, Progress in Astronautics and Aeronautics 153 (1993) 381–396.

[52] D. Bull, J. Elsworth, P. Shuff, E. Metcalfe, Detonation cell structures in fuel/air mixtures, Combustion and Flame 45 (1) (1982) 7–22.

[53] M. J. Kaneshige, Gaseous detonation initiation and stabilization by hypervelocity projectiles, Ph.D. thesis, California Institute of Technology (1999).

[54] W. Cao, D. Gao, H. Ng, J. Lee, Experimental investigation of near-limit gaseous detonations in small diameter spiral tubing, Proceedings of the Combustion Institute 37 (3) (2019) 3555–3563.

[55] J. Austin, The role of instability in gaseous detonation, Ph.D. thesis, California Institute of Technology (2003).

[56] P. Mach, M. Radulescu, Mach reflection bifurcations as a mechanism of cell multiplication in gaseous detonations, Proceedings of the Combustion Institute 33 (2) (2011) 2279–2285.

[57] A. Higgins, Steady one-dimensional detonations, Springer Berlin Heidelberg, Berlin, Heidelberg, 2012, pp. 33–105.

[58] J. Dionne, R. Duquette, A. Yoshinaka, J. Lee, Pathological detonations in H_2-Cl_2, Combustion Science and Technology 158 (1) (2000) 5–14.

[59] R. Mével, D. Davidenko, F. Lafosse, N. Chaumeix, G. Dupré, C. E. Paillard, J. E. Shepherd, Detonation in hydrogen-nitrous oxide-diluent mixtures: an experimental and numerical study, Combustion and Flame 162 (2015) 1638–1649.

[60] R. Mével, S. Pichon, L. Catoire, N. Chaumeix, C. E. Paillard, J. E. Shepherd, Dynamics of excited hydroxyl radicals in hydrogen-based mixtures behind reflected shock waves, Proceedings of the Combustion Institute 34 (1) (2013) 677–684.

[61] S. P. M. Bane, R. Mével, S. A. Coronel, J. E. Shepherd, Flame burning speeds of undiluted and nitrogen diluted hydrogen-nitrous oxide mixtures, International Journal of Hydrogen Energy 36 (2011) 10107–10116.